HHS Public Access

Author manuscript

*Biomaterials*. Author manuscript; available in PMC 2018 May 09.

Published in final edited form as:

*Biomaterials*. 2012 April ; 33(10): 2916–2925. doi:10.1016/j.biomaterials.2011.12.055.

# Biologic scaffold composed of skeletal muscle extracellular matrix

**Matthew T. Wolf**[a,b], **Kerry A. Daly**[b,c], **Janet E. Reing**[b], and **Stephen F. Badylak**[a,b,c,*]

[a]Department of Bioengineering, University of Pittsburgh, Pittsburgh, PA 15213, USA

[b]McGowan Institute for Regenerative Medicine, University of Pittsburgh, Pittsburgh, PA 15219, USA

[c]Department of Surgery, University of Pittsburgh, Pittsburgh, PA 15213, USA

## Abstract

Biologic scaffolds prepared from the extracellular matrix (ECM) of decellularized mammalian tissues have been shown to facilitate constructive remodeling in injured tissues such as skeletal muscle, the esophagus, and lower urinary tract, among others. The ECM of every tissue has a unique composition and structure that likely has direct effects on the host response and it is plausible that ECM harvested from a given tissue would provide distinct advantages over ECM harvested from nonhomologous tissues. For example, a tissue specific muscle ECM scaffold may be more suitable for constructive remodeling of skeletal muscle than non-homologous ECM tissue sources. The present study describes an enzymatic and chemical decellularization process for isolating skeletal muscle ECM scaffolds using established decellularization criteria and characterized the structure and chemical composition of the resulting ECM. The results were compared to those from a non-muscle ECM derived from small intestine (SIS). Muscle ECM was shown to contain growth factors, glycosaminoglycans, and basement membrane structural proteins which differed from those present in SIS. Myogenic cells survived and proliferated on muscle ECM scaffolds *in vitro*, and when implanted in a rat abdominal wall injury model *in vivo* was shown to induce a constructive remodeling response associated with scaffold degradation and myogenesis in the implant area; however, the remodeling outcome did not differ from that induced by SIS by 35 days post surgery. These results suggest that superior tissue remodeling outcomes are not universally dependent upon homologous tissue derived ECM scaffold materials.

### Keywords

ECM (extracellular matrix); Muscle; Scaffold; Regenerative medicine; Animal model

## 1. Introduction

Biologic scaffold materials composed of extracellular matrix (ECM) are typically produced by decellularization of mammalian tissues such as urinary bladder, dermis, or small intestine

*Corresponding author. McGowan Institute for Regenerative Medicine, 450 Technology Drive Suite 300, University of Pittsburgh, Pittsburgh, PA 15219, USA. Tel.: +1 412 624 5253; fax: +1 412 624 5256. badylaks@upmc.edu (S.F. Badylak).

[1] and have been shown to facilitate the functional reconstruction of several tissue types [2,3] including the lower urinary tract [4,5], heart and vascular structures [6,7], esophagus [8,9], and musculoskeletal tissues [10–13], among others. The mechanisms by which constructive remodeling occurs include the recruitment of multi-potential stem and progenitor cells to the site of scaffold placement [14,15], promotion of a favorable M2 macrophage phenotype at the host tissue/bioscaffold interface [16], regional angiogenesis [17], and mitogenesis [15,18]. These tissue derived biologic scaffolds are frequently used in non-homologous anatomic sites, but recent studies have suggested that biologic scaffolds derived from site specific homologous tissues such as liver and lung may be better suited for constructive tissue remodeling than non-site specific tissue sources [19–25].

Muscle tissues, including cardiac, skeletal, and smooth muscle, respond favorably when biologic scaffolds are used for their reconstruction following injury [11,12]. To date, there have been several attempts to isolate and process skeletal muscle ECM (M-ECM) [26–33]. Most of these attempts have involved the decellularization of intact rodent muscles or the extraction of rodent muscle ECM proteins, with varying degrees of success. DeQuach et al. [33] did show that proteins extracted from a decellularized porcine muscle matrix retain bioactivity. None of these studies have provided a detailed characterization of the intact M-ECM scaffold derived from a large animal tissue source, nor have any of these studies applied stringent decellularization criteria in the development of the decellularization process. The objectives of the present study were to (1) determine a method for decellularization of skeletal muscle and characterize the structure and composition of the resulting ECM, and (2) to compare the in-vitro bioactivity and in-vivo remodeling properties of skeletal muscle ECM vs. non-muscle ECM, specifically SIS, in a rodent model of abdominal wall muscle repair.

## 2. Materials and methods

### 2.1. Overview of study design

Canine skeletal muscle was harvested and decellularized by enzymatic and chemical methods. The resulting M-ECM was then assessed for biochemical and structural composition, the cell response *in vitro,* and the *in vivo* remodeling characteristics in a rat abdominal wall defect model. ECM composed of porcine small intestinal submucosa (SIS) was used for comparison purposes. All animal experiments were conducted in accordance to University of Pittsburgh Institutional Animal Care and Use Committee (IACUC) regulations and guidelines.

### 2.2. Preparation of M-ECM and SIS

Whole quadriceps and hamstring muscle groups were isolated from mongrel dogs and frozen at −80 °C immediately following sacrifice. While frozen, entire muscle groups were then sliced into 2.25 mm thick sheets transverse to the alignment of muscle fibers. The muscle slices were then thawed and trimmed of all macroscopic vasculature, fat, and connective tissues, rinsed in deionized water for 1 h and lyophilized.

The lyophilized muscle was decellularized following the protocol summarized in Table 1. Briefly, the muscle was subjected to lipid extraction by placement in a 2:1 (v/v) solution of chloroform/methanol (Fisher, Waltham, MA) for 2 h under a constant stir rate [34]. The muscle was rehydrated using a graded series of ethanol and then exposed to a series of enzymatic and chemical treatments to remove cellular materials in a spinner flask at a stir rate of 70RPM. These treatments consisted of: 0.2% Trypsin/0.2% EDTA for 2 h (at 37 °C and pH = 7.6), 2% sodium deoxycholate for 5 h, fresh 2% sodium deoxycholate for 14–16 h, 1% Triton-X 100 for 1 h, and finally 0.1% (w/v) peracetic acid/4% (v/v) ethanol for 2 h followed by extensive rinsing. The muscle tissue was washed with deionized water and 2× phosphate buffered saline (PBS) between each step. The M-ECM scaffolds were lyophilized for storage. Scaffolds used for tissue culture or *in vivo* implantation were terminally sterilized with ethylene oxide (16 h cycle at 50 °C in a Series 3plus EOGas Sterilizer, Anderson Sterilizers, Inc. Haw River, NC).

Porcine small intestine (jejunum) was obtained from 6 month old pigs from the local abbatoir and prepared as previously described [35]. In brief, the majority of the mucosa and the entire serosa, and muscularis externa layers of the intestine were mechanically delaminated from the intestine. The remaining submucosa, muscularis mucosa and stratum compactum layers were then washed with water and treated with 0.1% (w/v) peracetic acid/4% (v/v) ethanol for 1 h. SIS was then rinsed extensively, lyophilized, and sterilized with ethylene oxide.

### 2.3. Determination of decellularization

Decellularization was defined as fulfilling the following criteria for DNA content: having less than 50 ng dsDNA/mg ECM dry weight, having all residual DNA fragments be less than 200 base pair in size, and lacking visible nuclei after histologic staining with 4′,6-diamidino-2-phenylindole (DAPI) [1,36,37]. Immediately after processing, M-ECM samples ($n = 7$) were fixed in 10% neutral buffered formalin. Samples were then embedded in paraffin, surface sectioned, and then stained with H&E and DAPI for detection of nuclei multispectrally at 200× magnification. (Nuance multispectral imaging, CRi, Cambridge, MA) Additional non-fixed samples were used to quantify the amount of double stranded DNA using the PicoGreen assay (Invitrogen, Carlsbad, CA). DNA was extracted from powdered M-ECM by digesting in 0.1 mg/ml proteinase K (Sigma, St. Louis, MO) at 50 °C for 24 h. Samples were then purified with two phenol/chloroform/isoamyl alcohol (25:24:1 v/v) extractions. After ethanol precipitation and drying, the DNA was resuspended in 1 ml TE buffer (pH = 8.0) then quantified using the PicoGreen assay according to the manufacturer's instructions. The size of the extracted DNA fragments was determined after separation by 2% agarose gel electrophoresis.

### 2.4. Scanning electron microscopy

Scanning electron micrographs were taken to examine the surface topology of M-ECM and native muscle tissue. Prior to final lyophilization, samples were fixed in cold 2.5% (v/v) glutaraldehyde (Electron Microscopy Sciences, Hatfield, PA) in PBS for at least 24 h, followed by three washes in PBS. Lipid fixation was performed in 1% (w/v) osmium tetroxide (Electron Microscopy Sciences) for 1 h followed by three washes in PBS. Fixed

samples were then dehydrated using a graded series of alcohol (30, 50, 70, 90, 100%) for 15 min each, followed by 15 min in hexamethylenediamine (Fisher) and subsequent air drying. The dried samples were sputter coated with a 3.5 nm layer of gold/palladium alloy using a Sputter Coater 108 Auto (Cressington Scientific Instruments, Watford, UK) and imaged with a JEOL JSM6330f scanning electron microscope (JEOL, Peabody, MA) at 25×, 500×, 1000×, and 10,000× magnifications.

### 2.5. Sulfated glycosaminoglycan quantification

Sulfated glycosaminoglycan (GAG) content in different preparations of M-ECM ($n = 7$), SIS ($n = 4$), and native muscle tissue ($n = 3$) was determined using the Blyscan Sulfated Glycosaminoglycan Assay Kit (Biocolor Life Sciences, Carrickfergus, UK). For each sample, 25 mg/ml of powdered ECM in 100 mM Tris (pH = 7.5) was digested with 0.1 mg/ml proteinase K (Sigma) at 50 °C for 24 h with gentle agitation. The digested scaffold was then assayed following the manufacturer's instructions.

### 2.6. Protein extraction & growth factor quantification

Soluble proteins were extracted from different preparations of M-ECM ($n = 5$), SIS ($n = 3$), and native muscle tissue ($n = 2$) and analyzed for growth factor content. Soluble proteins were extracted from 300 mg of powdered ECM or tissue in 7 ml of a urea-heparin buffer (2M urea, 50 mM Tris, 5 mg/ml heparin, 10 mM N-ethyl-maleimide, 5 mM benzamidine, and 1 mM phenylmethylsulfonyl fluoride at pH = 7.4). Samples in urea-heparin buffer were gently agitated for 20–24 h at 4 °C, after which they were centrifuged for 30 min at 3000*g* and the supernatant collected. The remaining pellet was resuspended in freshly prepared urea-heparin buffer and the extraction process repeated. Each extract was then dialyzed against 80–100× volume of deionized water using 3500MWCO Slide-A-Lyzer dialysis cassettes (Pierce, Rockford, IL) for 24 h, with water changes after 4 and 8 h. The recovered extracts were analyzed for total protein recovered using the BCA protein assay (Pierce) and frozen at −80 °C until further use.

The isolated protein extracts were quantified for vascular endothelial growth factor (VEGF) and basic fibroblast growth factor (bFGF) with human ELISAs (R&D systems, Minneapolis, MN) following the manufacturer's instructions. Canine, porcine, and human bFGF and VEGF show a high level of sequence homology and extractions from native canine tissue were found to be reactive with the human ELISA kits used.

### 2.7. ECM staining and immunolabeling

M-ECM, SIS, and native muscle tissue were fixed in formalin, embedded in paraffin, and then cut into 5 μm sections. Standard histologic stains were performed using Herovici's Polychrome (staining for collagen Types I & III) and Movat's Pentachrome (staining for elastin, collagen, and GAGs). Immunolabeling studies were also conducted for the presence of basement membrane proteins laminin, type IV collagen, and fibronectin.

For immunolabeling, slides were deparaffinized followed by epitope retrieval in 10 mM citrate buffer (pH = 6.0) at 95 °C for 15 min. Endogenous peroxidase activity was quenched by incubation in a 3% (v/v) hydrogen peroxide/methanol solution for 30 min at room

temperature. Non-specific antibody binding was blocked with 2% normal goat serum in PBS (Vector, Burlingame, CA) for 1 h at room temperature. Tissues were then labeled with primary antibodies overnight at 4 °C. Antibodies were raised in rabbit against human laminin (1:50, L9393, Sigma), type IV collagen (1:100, T59106R, Meridian Life Science Inc., Saco, ME), and fibronectin (1:300, F3648, Sigma) and were diluted in the blocking solution. Sections were then rinsed in PBS and incubated in a biotinylated goat anti-rabbit IgG secondary antibody (1:100, Vector) diluted in blocking solution for 2 h at room temperature. Sections were rinsed as before and incubated in the Vectastain ABC reagent (Vector) for 30 min at room temperature and then exposed to a diaminobenzadine substrate (ImmPact DAB, Vector) until appropriate staining developed. Staining was stopped by rinsing sections in deionized water followed by counterstaining with hematoxylin. Antibody isotype controls were used in the place of the primary antibody to determine the presence of non-specific staining.

### 2.8. Cell culture on M-ECM scaffolds

C2C12 mouse myoblast, human perivascular stem cell, NIH 3T3 mouse fibroblast, and human microvascular endothelial cell (HMEC) lines were cultured on the surface of M-ECM scaffolds and the abluminal side of SIS to evaluate *in vitro* cell compatibility. The perivascular stem cells were isolated from fetal skeletal muscle (as described by Crisan et al. [38]), and passage 8–12 was utilized for all experiments. The HMEC, C2C12, and NIH 3T3 cell lines were obtained from ATCC (Manassas, VA). C2C12 and NIH 3T3 cells were cultured in Dulbecco's Modified Eagle Medium (DMEM) (Invitrogen) supplemented with 10% fetal bovine serum (FBS), (Hyclone) and 100 U/ml penicillin/100 μg/ml streptomycin (Invitrogen). HMECs were cultured in MDCB131 Medium (Invitrogen), supplemented with 10% FBS and 100 U/ml penicillin/100 μg/ml streptomycin. Perivascular stem cells were cultured in DMEM supplemented with 20% FBS and 100 U/ml penicillin/100 μg/ml streptomycin. C2C12 cells were also cultured in low serum conditions to induce myotube formation, which consisted of DMEM supplemented with 2% horse serum and 100 U/ml penicillin/100 μg/ml streptomycin.

C2C12 cells, perivascular stem cells, NIH 3T3 cells, and HMEC cells were seeded on the surface of lyophilized sheets of M-ECM at a density of 500,000 cells/cm$^2$ for 7 days, with media changes after the 1st and 4th days. C2C12 cells were grown in both high serum and low serum differentiation conditions. The cell seeded scaffolds were then fixed in formalin, cut into 5 μm cross sections, and stained with H&E. These were imaged at 200× magnification and evaluated for cell morphology characteristics. Perivascular stem cell seeded scaffolds were also fixed with formalin and labeled with Alexa Fluor-546 conjugated phalloidin (Invitrogen) for actin and DAPI for nuclei. The scaffold surface was then imaged with a confocal microscope. (Leica DMI 4000B, Leica Microsystems, Buffalo Grove, IL).

### 2.9. Cell metabolism on M-ECM scaffolds

Lyophilized M-ECM and SIS sheets ($n$ = 6–12) from 2 different scaffold preparations were cut into 8 mm disks using a biopsy hole punch, placed into a 96-well plate, and anchored to the bottom of the wells with silicone rings. The disks were sterilized with ethylene oxide (16 h cycle at 50 °C in a Series 3plus EOGas Sterilizer) and seeded in triplicate with C2C12

myoblasts or perivascular stem cells at a density of 4000 cells/well in 200 μl of media. Cells were also seeded in wells with only the plastic anchor ring as controls ($n$ = 3–6). Cells were cultured for 1, 3, and 5 days in standard media, and at each timepoint, cell metabolism was assessed using the alamar blue assay (Invitrogen). Alamar Blue reagent was added to each well for 6 h, then transferred to a separate plate and read fluorescently (ex:560, em:590). A non-seeded scaffold background control was subtracted from each reading. All values were normalized to a standard curve of 1000–20,000 cells/well adding Alamar Blue 4 h after seeding and measuring after 6 h of incubation in the Alamar Blue reagent.

### 2.10. In vivo implantation of M-ECM scaffolds in a rat abdominal wall defect

The *in vivo* remodeling characteristics of M-ECM and SIS scaffolds were determined in a partial thickness abdominal wall defect model in the rat [11,17]. A 1 × 1 cm partial thickness defect was created in the ventrolateral abdominal wall of female Sprague–Dawley rats by removing the external and internal oblique muscles (both are skeletal muscle) while leaving the transversalis muscle and the peritoneum intact. The defect was repaired with a 1 × 1 cm sheet of M-ECM or SIS sutured at the 4 corners of the defect with 4-0 Prolene sutures (Ethicon Inc., Somerville, NJ), or left untreated with no implanted ECM as a defect only control. The skin incision was then closed with absorbable 4-0 Vicryl sutures (Ethicon) and the rats were allowed to recover normally. Rats were sacrificed 14 and 35 days post-implantation ($n$ = 4 per group per timepoint), and the repaired defects were excised and fixed with formalin. Explants were then embedded in paraffin, sectioned, and stained with Masson's Trichrome stain or immunolabeled for fast and slow myosin heavy chain (MHC) to evaluate myogenesis as previously described [11]. Slides were deparaffinized followed by epitope retrieval in 0.1 mM EDTA at 95–100 °C for 25 min and then 0.1% Trypsin/0.1% Calcium Chloride (w/v) at 37 °C for 10 min. Endogenous peroxidase activity was quenched by incubation in a 0.3% (v/v) hydrogen peroxide solution in TBS for 10 min at room temperature. Sections were then blocked with 2% normal horse serum/1% BSA in TBS (Vector) for 30 min at room temperature and then labeled with mouse anti-slow myosin heavy chain (1:1000, M8421, Sigma) for 40 min at room temperature. Sections were then rinsed in TBS and incubated in a biotinylated goat anti-mouse IgG secondary antibody (1:200, Vector) diluted in blocking solution for 1 h at room temperature. Sections were washed as before and incubated in the Vectastain ABC reagent (Vector) for 30 min at room temperature and then exposed to a diaminobenzadine substrate (ImmPact DAB, Vector) until appropriate staining developed. Sections were then incubated in blocking solution for 10 min followed by incubation in alkaline phosphatase conjugated mouse anti-fast myosin heavy chain (1:200, A4335, Sigma) diluted in blocking solution for 1 h. After rinsing, color was developed by staining with red alkaline phosphatase (Vector) until appropriate staining developed. Slides were then counterstained with hematoxylin, dehydrated, and cover slipped.

### 2.11. Statistical analysis

All statistical analysis was performed using MATLAB software (MathWorks, Natick, MA). Differences in composition (GAGs, total protein, bFGF, and VEGF) comparing M-ECM to SIS or native muscle tissue were found using a two-tailed Student's $t$-test with a significance level of $p < 0.05$. Metabolic activity differences were determined for both C2C12 myoblast

and perivascular stem cell seeded scaffolds. Each substrate at every time point was analyzed using a two-way analysis of variance (ANOVA) with a Tukey post-hoc test and with a significance level of $p < 0.05$. All values are given as the mean ± standard deviation.

## 3. Results

### 3.1. Verification of decellularization

The amount and size of residual DNA content after decellularization for each preparation of M-ECM prepared was quantified and is presented in Fig. 1. Histologic analysis of M-ECM (Fig. 1A and C) showed no evidence of intact nuclear material on H&E or DAPI as compared to native muscle (Fig. 1B and D). After decellularization, there was 7.42 + 1.67 ng DNA/mg dry weight compared to the 1549 ± 489 ng DNA/mg dry weight found in native muscle tissue (Fig. 1E). There were no clearly visible bands of DNA after separation on a 2% agarose gel, while native muscle showed a range of DNA fragments (Fig. 1F). These values met previously described criteria of decellularization [1,36,37].

### 3.2. Scanning electron microscopy

The surface topology of M-ECM scaffolds was compared to native muscle tissue using SEM and is presented in Fig. 2. M-ECM had an uneven surface composed of compact structures in a net like pattern (Fig. 2A–D). Higher magnification revealed that these structures consisted of long compact fibrils or bundles of fibrils with a banding pattern suggestive of collagen (Fig. 2D, arrows). No myofiber cellular remnants were seen. In contrast, native muscle showed clear tubular myofiber boundaries with densely packed microfibrillar elements within each cell (Fig. 2E–F).

### 3.3. Sulfated glycosaminoglycan quantification

The results of the GAG assay are summarized in Fig. 3A. M-ECM contained 0.61 ± 0.01 μg/mg dry weight of sulfated GAGs after decellularization compared to the 3.02 ± 0.56 μg/mg dry weight in native muscle tissue. SIS had the greatest amount of GAGs with 9.97 + 0.58 μg/mg dry weight.

### 3.4. Protein & growth factor quantification

Soluble proteins remaining in M-ECM, SIS, and native muscle were extracted using urea-heparin extraction buffer and then were quantified using the BCA protein assay as summarized in Fig. 3B. The amount of protein extracted from M-ECM was 2.30 ± 0.57 mg protein/g dry weight for M-ECM, which was two orders of magnitude less than the 203.03 ± 30.74 extracted from native muscle tissue and one order of magnitude less than the 23.04 ± 2.52 extracted from SIS.

Total amounts of bFGF are presented in Fig. 3C. M-ECM retained bFGF, though in lower amounts than SIS. Total bFGF content was found to be 10.15 ± 2.34 ng bFGF/g dry weight in M-ECM, which was less than the 75.22 ± 19.57 found in SIS and the 31.41 ± 8.28 ng bFGF/g dry weight found in native muscle. When normalizing these bFGF values to the amount of total protein extracted in Fig. 3D, M-ECM, SIS, and native muscle were similar with 6.85 ± 2.56, 3.61 ± 1.37, and 0.20 ± 0.088 ng bFGF/mg protein, respectively. There

was no detectable VEGF extracted from M-ECM or SIS. Native muscle contained 56.10 ± 12.93 ng VEGF/g dry weight.

### 3.5. ECM staining and immunolabeling

M-ECM scaffolds and native muscle was stained with Herovici's and Movat's Pentachrome stains as shown in Fig. 4. Herovici's staining of native muscle showed a distribution of thick type I collagen in the perimysium (purple) and type III collagen staining (blue) around individual muscle fibers consistent with previous studies (Fig. 4A) [39]. Herovici's staining of M-ECM showed thick Type I collagen bundles and dispersed strands of Type III collagen (Fig. 4B). Movat's pentachrome showed the presence of collagen (yellow) in the perimysium of native muscle (Fig. 4C) and in M-ECM (Fig. 4D). M-ECM also shows positive elastin staining (black, Fig. 4D), which is localized to long strands that are possible remnants of blood vessels.

M-ECM scaffolds and native muscle tissue showed evidence of basement membrane proteins laminin, type IV collagen, and fibronectin (Fig. 5). In native muscle, there was a clear localization of laminin and type IV collagen to the basement membrane surrounding muscle fibers (Figure 5A–B). Fibronectin was found on basement membranes of native muscle as well as the interstitial connective tissue (Fig. 5C). SIS showed no positive laminin staining, but prevalent type IV collagen and fibronectin staining (Fig. 5G–I). Antibody isotype controls verified the lack of non-specific staining (data not shown).

### 3.6. Cell culture and compatibility on M-ECM scaffolds

Cell attachment, survival, and morphology was assessed using histologic methods for M-ECM and SIS scaffolds seeded with the following cell lines for 7 days in culture: C2C12 myoblasts (Fig. 6A & B), human perivascular stem cells (Fig. 6C–E), NIH 3T3 fibroblasts, HMEC endothelial cells, and differentiated C2C12 myotubes (Supplementary Fig. 1). Histologic cross sections showed a confluent layer of cells on the surface that possessed a normal, healthy morphology for all cell types on both M-ECM and SIS. Normal cell morphology was further confirmed for perivascular stem cells by staining and imaging the surface with phalloidin for actin (Fig. 6E) showing spread cell morphology forming a confluent monolayer. C2C12 differentiation was supported on both M-ECM (Supplementary Figs. 1E & F) with the presence of elongated multi-nucleate myotubes upon histologic examination.

### 3.7. Cell metabolism on M-ECM

The proliferation of C2C12 myoblasts (Fig. 7A) and perivascular stem cells (Fig. 7B) seeded on M-ECM and SIS scaffolds or seeded in empty wells (TC) was estimated from the Alamar Blue assay and all differences defined as $p < 0.05$. C2C12 metabolic activity was greater on seeded TC than SIS from day 1 onward, and greater than M-ECM from day 3 on. M-ECM metabolic activity did not change over the time course of the study, but SIS and TC showed an increase from day 1 at days 5 and 3, respectively. In contrast, perivascular stem cells seeded on TC did not show alterations in metabolic activity over the time course of the study. Both M-ECM and SIS seeded scaffolds showed an increase in cell metabolism between days 1 and 5.

### 3.8. In vivo implantation of M-ECM scaffolds in a rat abdominal wall defect

M-ECM and SIS sheets were implanted in a partial thickness abdominal wall defect for 14 and 35 days and evaluated by histologic methods. At 14 days, both M-ECM and SIS scaffolds showed a robust mononuclear cell response with a dense accumulation of cells around the implants (Fig. 8A–D). Compared to M-ECM, the SIS scaffold displayed a greater extent of degradation as shown by a highly fragmented scaffold appearance at 14 days (Fig. 8B and D, asterisks). There were occasional multinucleate cells in direct contact with the M-ECM scaffold (Fig. 8B, arrowheads) that was absent in the SIS group. Both implants showed angiogenesis around the scaffolds (Fig. 8B and D). By 35 days, the mononuclear cell response had largely dissipated in both scaffolds and there was evidence of myogenesis within a more organized collagenous connective tissue (Fig. 8E–H). For M-ECM, there were still scattered regions in which the scaffold had not completely degraded, with collagenous bands of scaffold visible on histologic examination (Fig. 9A, asterisks) with associated multinucleate cells (Fig. 9A, arrowheads). The SIS scaffold was more completely degraded, with the infrequent exception of scattered small fragments (Fig. 9B, asterisks) surrounded by a dense accumulation of mononuclear cells. Islands of small diameter muscle fibers staining positive for slow or fast myosin heavy chain were occasionally found in the defect at the interface with the subjacent transversalis fascia (Figure 8I–L). A greater proportion of the muscle stained positive for fast myosin than slow, consistent with the staining pattern in adjacent native muscle. There was no apparent difference in the amount or phenotype of new muscle observed between M-ECM and SIS scaffolds at the 35 day timepoint. The unrepaired defect only control group at 35 days showed only a thin layer of collagenous connective tissue within the defect area, and little evidence of continued remodeling. (Supplementary Fig. 2A & B) There was a dispersed spindle shaped cell population and no observed myogenic cells.

## 4. Discussion

A method for the preparation of skeletal muscle ECM scaffolds from a large animal tissue source is described in the present study. The M-ECM scaffold was shown to be thoroughly decellularized by established criteria while simultaneously preserving many of the components found in the native ECM. The bioactivity of the scaffold was evaluated and shown to affect the proliferative potential of muscle progenitor cells *in vitro* as well as the induction of a constructive remodeling response *in vivo*. Although differences were identified in the structure and composition of the ECM scaffolds prepared from skeletal muscle and small intestinal submucosa, no differences were present in their respective effects upon the remodeling of skeletal muscle in a rodent model.

The method of preparation of an ECM scaffold can have profound effects upon the composition, ultrastructure, and subsequent host response to the scaffold following implantation. Skeletal muscle ECM scaffolds have been prepared and evaluated for the purpose of *in vivo* skeletal muscle reconstruction and several different decellularization approaches have been described. Merritt et al. provided a detailed assessment of the *in vivo* host response to acellular skeletal muscle and observed myogenesis at the scaffold/tissue interface, but found functional recovery only when mesenchymal stem cells were pre-seeded

on the scaffold [30,40]. This study utilized a relatively harsh decellularization protocol compared to methods described in the present study. Such harsh methods are effective at removing cellular material but also effectively denature matrix components [41,42]. Other studies have reported the use of decellularized muscle tissue with less harsh decellularization protocols; however, quantification of decellularization was not attempted. While most visible nuclear material can be removed following decellularization attempts, cell remnants remain within the matrix, which can adversely affect *in vivo* remodeling. Consequently, less than ideal remodeling responses occur *in vivo* with the exception of those scaffolds pre-seeded with myogenic cells [26–29].

Although most clinical applications of ECM scaffolds have involved a non-homologous implantation site, there have been recent studies which suggest an advantage for the use of site specific ECM [19–24,43,44]. The concept of tissue specificity in ECM scaffolds is predicated upon the concept that there is a unique structure and composition within each tissue, and even within different regions of individual tissues. The ECM of tissues and organs provides a microenvironmental niche for resident cells that promotes and maintains site appropriate phenotype and function [45]. This niche environment is the sum of both structural and biochemical milieu that includes collagens, glycosaminoglycans, proteoglycans, and bound growth factors, among others that may influence myogenesis and the remodeling response [46].

The M-ECM characterized in the present study maintains several of the factors found in native muscle tissue including basement membrane proteins and GAGs. Growth factors can be sequestered within the ECM, and FGF was shown in the present study to survive the decellularization process. Although assays used in the present study do not determine biologic activity, previous studies have shown that growth factors within decellularized tissues can stimulate cells in culture [47]. The differences in composition between M-ECM and SIS in the present study are most likely explained by not only the different tissue sources (muscle vs. small intestine), but also by the different decellularization techniques that were used. SIS is a thin material prepared primarily by mechanical methods from the parent small intestine tissue and a brief exposure to peracetic acid. M-ECM on the other hand uses enzymatic and detergent chemical methods that have different effects upon the matrix.

In addition to the retention of components found in the native ECM, M-ECM was shown to be cell compatible for a number of cell types *in vitro* as evaluated using histologic methods and with the Alamar Blue assay. C2C12 cells seeded on M-ECM and SIS were similar in their metabolic profile over the time course of the study, which was less than in non-ECM covered wells. Perivascular stem cells, however, showed greater growth over time compared to non-ECM covered cells. These effects may have been due to the presence of ECM specific attachment proteins, or soluble growth factors that may have eluted from the scaffold during culture. It should be noted that the Alamar Blue assay is a metabolic assay, which is not directly correlated to cell number in all circumstances.

The determinants of success for biologic scaffold remodeling *in vivo* are not fully understood, but empirical observations have proven informative. SIS that is prepared without

chemical cross-linking has been shown to promote a constructive remodeling response, myogenesis, and partial restoration of function [11,12]. Thoroughness of decellularization, as attained in the present study, avoids a proinflammatory response whereas ineffective decellularization is associated with a robust inflammatory response [48]. ECM scaffold degradation is another determinant of remodeling outcome. Degradation products of ECM scaffolds have been shown to have chemotactic and mitogenic effects on stem cells *in vitro* and *in vivo* [15,18], and inhibition of scaffold degradation is associated with less desirable outcomes [11,17]. M-ECM, like SIS and other previously evaluated scaffolds, invokes a strong cellular response at early timepoints, which dissipates over time in a partial thickness abdominal wall defect model. M-ECM showed a morphologically different cell population, specifically, multinucleate cells, in direct contact with the scaffold at 14 days. Multinucleate cells were not seen in the tissue response to the SIS-ECM scaffold. M-ECM did appear to degrade more slowly than SIS, with some intact M-ECM scaffold fragments visible at 35 days. There was extensive remodeling in areas where the M-ECM had degraded, with small islands of myosin heavy chain expressing muscle cells in the defect area in a very similar pattern to SIS at this time point. In contrast, the unrepaired defect only control, exhibited very little remodeling and no myogenesis confirming the positive influence of M-ECM and SIS scaffolds on the host response. Despite the numerous differences in the structure, composition, and early host responses between M-ECM and SIS, the remodeling characteristics and myogenesis at 35 days were indistinguishable. It is possible that there will be additional divergence in the remodeling outcome at later time points when remodeling is complete. Future studies will evaluate M-ECM in a larger defect model to better evaluate myogenesis over longer periods of time and also evaluate functionality of any new muscle tissue that may occur during the remodeling process.

## 5. Conclusions

A M-ECM scaffold can be prepared from a large animal source using an enzymatic and chemical processing method. The M-ECM conforms with established decellularization criteria while preserving factors found in native muscle ECM that may be beneficial to the host remodeling response. The M-ECM exerts biologic effects on myogenic cells *in vitro* and promotes positive remodeling characteristics in a rodent muscle defect model. However, when compared to the nonhomologous SIS there was no detectable advantage in using a tissue specific M-ECM scaffold, despite differences in the structure and composition of the two bioscaffold materials.

## Supplementary Material

Refer to Web version on PubMed Central for supplementary material.

## Acknowledgments

Funding for this work was provided by the Advanced Regenerative Medicine (ARM III) grant W81XWH-07-1-0415. Matthew Wolf was partially supported by the NIH-NHLBI training grant (T32-HL76124-6) entitled “Cardiovascular Bioengineering Training Program” through the University of Pittsburgh Department of Bioengineering. The authors would like to thank Deanna Rhoads and the McGowan Histology Center for histologic section preparation, the Center for Biologic Imaging at the University of Pittsburgh for access to imaging facilities, and Jonathan Franks for scanning electron micrograph interpretation.

## References


1. Crapo PM, Gilbert TW, Badylak SF. An overview of tissue and whole organ decellularization processes. Biomaterials. 2011; 32(12):3233–43. [PubMed: 21296410]
2. Badylak SF. The extracellular matrix as a biologic scaffold material. Biomaterials. 2007; 28(25): 3587–93. [PubMed: 17524477]
3. Song JJ, Ott HC. Organ engineering based on decellularized matrix scaffolds. Trends Mol Med. 2011; 17(8):424–32. [PubMed: 21514224]
4. Boruch AV, Nieponice A, Qureshi IR, Gilbert TW, Badylak SF. Constructive remodeling of biologic scaffolds is dependent on early exposure to physiologic bladder filling in a canine partial cystectomy model. J Surg Res. 2009; 161(2):217–25. [PubMed: 19577253]
5. Reddy PP, Barrieras DJ, Wilson G, Bagli DJ, McLorie GA, Khoury AE, et al. Regeneration of functional bladder substitutes using large segment acellular matrix allografts in a porcine model. J Urol. 2000; 164(3 Pt 2):936–41. [PubMed: 10958712]
6. Quarti A, Nardone S, Colaneri M, Santoro G, Pozzi M. Preliminary experience in the use of an extracellular matrix to repair congenital heart disases. Interact Cardiovasc Thorac Surg. 2011; 6:569–72.
7. Badylak SF, Kochupura PV, Cohen IS, Doronin SV, Saltman AE, Gilbert TW, et al. The use of extracellular matrix as an inductive scaffold for the partial replacement of functional myocardium. Cell Transplant. 2006; 15(Suppl 1):S29–40. [PubMed: 16826793]
8. Desai KM, Diaz S, Dorward IG, Winslow ER, La Regina MC, Halpin V, et al. Histologic results 1 year after bioprosthetic repair of paraesophageal hernia in a canine model. Surg Endosc. 2006; 20(11):1693–7. [PubMed: 17031737]
9. Badylak SF, Vorp DA, Spievack AR, Simmons-Byrd A, Hanke J, Freytes DO, et al. Esophageal reconstruction with ECM and muscle tissue in a dog model. J Surg Res. 2005; 128(1):87–97. [PubMed: 15922361]
10. Franklin ME Jr, Trevino JM, Portillo G, Vela I, Glass JL, Gonzalez JJ. The use of porcine small intestinal submucosa as a prosthetic material for laparoscopic hernia repair in infected and potentially contaminated fields: long-term follow-up. Surg Endosc. 2008; 22(9):1941–6. [PubMed: 18594919]
11. Valentin JE, Turner NJ, Gilbert TW, Badylak SF. Functional skeletal muscle formation with a biologic scaffold. Biomaterials. 2010; 31(29):7475–84. [PubMed: 20638716]
12. Turner NJ, Yates AJ Jr, Weber DJ, Qureshi IR, Stolz DB, Gilbert TW, et al. Xenogeneic extracellular matrix as an inductive scaffold for regeneration of a functioning musculotendinous junction. Tissue Eng Part A. 2010; 16(11):3309–17. [PubMed: 20528669]
13. Smith MJ, Paran TS, Quinn F, Corbally MT. The SIS extracellular matrix scaffold-preliminary results of use in congenital diaphragmatic hernia (CDH) repair. Pediatr Surg Int. 2004; 20(11–12): 859–62. [PubMed: 15565305]
14. Beattie AJ, Gilbert TW, Guyot JP, Yates AJ, Badylak SF. Chemoattraction of progenitor cells by remodeling extracellular matrix scaffolds. Tissue Eng Part A. 2009; 15(5):1119–25. [PubMed: 18837648]
15. Reing JE, Zhang L, Myers-Irvin J, Cordero KE, Freytes DO, Heber-Katz E, et al. Degradation products of extracellular matrix affect cell migration and proliferation. Tissue Eng Part A. 2009; 15(3):605–14. [PubMed: 18652541]
16. Brown BN, Valentin JE, Stewart-Akers AM, McCabe GP, Badylak SF. Macrophage phenotype and remodeling outcomes in response to biologic scaffolds with and without a cellular component. Biomaterials. 2009; 30(8):1482–91. [PubMed: 19121538]
17. Valentin JE, Badylak JS, McCabe GP, Badylak SF. Extracellular matrix bio-scaffolds for orthopaedic applications. A comparative histologic study. J Bone Jt Surg Am. 2006; 88(12):2673–86.
18. Vorotnikova E, McIntosh D, Dewilde A, Zhang J, Reing JE, Zhang L, et al. Extracellular matrix-derived products modulate endothelial and progenitor cell migration and proliferation in vitro and stimulate regenerative healing in vivo. Matrix Biol. 2010; 29(8):690–700. [PubMed: 20797438]

19. Cortiella J, Niles J, Cantu A, Brettler A, Pham A, Vargas G, et al. Influence of acellular natural lung matrix on murine embryonic stem cell differentiation and tissue formation. Tissue Eng Part A. 2010; 16(8):2565–80. [PubMed: 20408765]
20. Sellaro TL, Ravindra AK, Stolz DB, Badylak SF. Maintenance of hepatic sinusoidal endothelial cell phenotype in vitro using organ-specific extracellular matrix scaffolds. Tissue Eng. 2007; 13(9):2301–10. [PubMed: 17561801]
21. Zhang Y, He Y, Bharadwaj S, Hammam N, Carnagey K, Myers R, et al. Tissue-specific extracellular matrix coatings for the promotion of cell proliferation and maintenance of cell phenotype. Biomaterials. 2009; 30(23–24):4021–8. [PubMed: 19410290]
22. Ott HC, Clippinger B, Conrad C, Schuetz C, Pomerantseva I, Ikonomou L, et al. Regeneration and orthotopic transplantation of a bioartificial lung. Nat Med. 2010; 16(8):927–33. [PubMed: 20628374]
23. Cheng NC, Estes BT, Awad HA, Guilak F. Chondrogenic differentiation of adipose-derived adult stem cells by a porous scaffold derived from native articular cartilage extracellular matrix. Tissue Eng Part A. 2009; 15(2):231–41. [PubMed: 18950290]
24. Uygun BE, Soto-Gutierrez A, Yagi H, Izamis ML, Guzzardi MA, Shulman C, et al. Organ reengineering through development of a transplantable recellularized liver graft using decellularized liver matrix. Nat Med. 2010; 16(7):814–20. [PubMed: 20543851]
25. Petersen TH, Calle EA, Zhao L, Lee EJ, Gui L, Raredon MB, et al. Tissue-engineered lungs for in vivo implantation. Science. 2010; 329(5991):538–41. [PubMed: 20576850]
26. Conconi MT, Bellini S, Teoli D, de Coppi P, Ribatti D, Nico B, et al. In vitro and in vivo evaluation of acellular diaphragmatic matrices seeded with muscle precursors cells and coated with VEGF silica gels to repair muscle defect of the diaphragm. J Biomed Mater Res A. 2009; 89(2):304–16. [PubMed: 18431788]
27. Conconi MT, De Coppi P, Bellini S, Zara G, Sabatti M, Marzaro M, et al. Homologous muscle acellular matrix seeded with autologous myoblasts as a tissue-engineering approach to abdominal wall-defect repair. Biomaterials. 2005; 26(15):2567–74. [PubMed: 15585259]
28. De Coppi P, Bellini S, Conconi MT, Sabatti M, Simonato E, Gamba PG, et al. Myoblast-acellular skeletal muscle matrix constructs guarantee a long-term repair of experimental full-thickness abdominal wall defects. Tissue Eng. 2006; 12(7):1929–36. [PubMed: 16889522]
29. Gamba PG, Conconi MT, Lo Piccolo R, Zara G, Spinazzi R, Parnigotto PP. Experimental abdominal wall defect repaired with acellular matrix. Pediatr Surg Int. 2002; 18(5–6):327–31. [PubMed: 12415348]
30. Merritt EK, Hammers DW, Tierney M, Suggs LJ, Walters TJ, Farrar RP. Functional assessment of skeletal muscle regeneration utilizing homologous extracellular matrix as scaffolding. Tissue Eng Part A. 2010; 16(4):1395–405. [PubMed: 19929169]
31. Stern MM, Myers RL, Hammam N, Stern KA, Eberli D, Kritchevsky SB, et al. The influence of extracellular matrix derived from skeletal muscle tissue on the proliferation and differentiation of myogenic progenitor cells ex vivo. Biomaterials. 2009; 30(12):2393–9. [PubMed: 19168212]
32. Gillies AR, Smith LR, Lieber RL, Varghese S. Method for decellularizing skeletal muscle without detergents or proteolytic enzymes. Tissue Eng Part C Methods. 2011; 17(4):383–9. [PubMed: 20973753]
33. DeQuach JA, Mezzano V, Miglani A, Lange S, Keller GM, Sheikh F, et al. Simple and high yielding method for preparing tissue specific extracellular matrix coatings for cell culture. PLoS One. 2010; 5(9):e13039. [PubMed: 20885963]
34. Kurihara T, Nishizawa Y, Takahashi Y. The use of non-aqueous chloroform/methanol extraction for the delipidation of brain with minimal loss of enzyme activities. Biochem J. 1977; 165(1):135–40. [PubMed: 196593]
35. Lantz GC, Badylak SF, Coffey AC, Geddes LA, Sandusky GE. Small intestinal submucosa as a superior vena cava graft in the dog. J Surg Res. 1992; 53(2):175–81. [PubMed: 1405606]
36. Daly KA, Stewart-Akers AM, Hara H, Ezzelarab M, Long C, Cordero K, et al. Effect of the alphaGal epitope on the response to small intestinal submucosa extracellular matrix in a nonhuman primate model. Tissue Eng Part A. 2009; 15(12):3877–88. [PubMed: 19563260]

37. Reing JE, Brown BN, Daly KA, Freund JM, Gilbert TW, Hsiong SX, et al. The effects of processing methods upon mechanical and biologic properties of porcine dermal extracellular matrix scaffolds. Biomaterials. 2010; 31(33):8626–33. [PubMed: 20728934]
38. Crisan M, Yap S, Casteilla L, Chen CW, Corselli M, Park TS, et al. A perivascular origin for mesenchymal stem cells in multiple human organs. Cell Stem Cell. 2008; 3(3):301–13. [PubMed: 18786417]
39. Light N, Champion AE. Characterization of muscle epimysium, perimysium and endomysium collagens. Biochem J. 1984; 219(3):1017–26. [PubMed: 6743238]
40. Merritt EK, Cannon MV, Hammers DW, Le LN, Gokhale R, Sarathy A, et al. Repair of traumatic skeletal muscle injury with bone-marrow-derived mesenchymal stem cells seeded on extracellular matrix. Tissue Eng Part A. 2010; 16(9):2871–81. [PubMed: 20412030]
41. Gratzer PF, Harrison RD, Woods T. Matrix alteration and not residual sodium dodecyl sulfate cytotoxicity affects the cellular repopulation of a decellularized matrix. Tissue Eng. 2006; 12(10): 2975–83. [PubMed: 17518665]
42. Otzen D. Protein-surfactant interactions: a tale of many states. Biochim Biophys Acta. 2011; 1814(5):562–91. [PubMed: 21397738]
43. Soto-Gutierrez A, Zhang L, Medberry C, Fukumitsu K, Faulk D, Jiang H, et al. A whole-organ regenerative medicine approach for liver replacement. Tissue Eng Part C Methods. 2011; 17(6): 677–86. [PubMed: 21375407]
44. Macchiarini P, Jungebluth P, Go T, Asnaghi MA, Rees LE, Cogan TA, et al. Clinical transplantation of a tissue-engineered airway. Lancet. 2008; 372(9655):2023–30. [PubMed: 19022496]
45. Fuchs E, Tumbar T, Guasch G. Socializing with the neighbors: stem cells and their niche. Cell. 2004; 116(6):769–78. [PubMed: 15035980]
46. Kuang S, Kuroda K, Le Grand F, Rudnicki MA. Asymmetric self-renewal and commitment of satellite stem cells in muscle. Cell. 2007; 129(5):999–1010. [PubMed: 17540178]
47. Hodde J, Janis A, Ernst D, Zopf D, Sherman D, Johnson C. Effects of sterilization on an extracellular matrix scaffold: part I. Composition and matrix architecture. J Mater Sci Mater Med. 2007; 18(4):537–43. [PubMed: 17546412]
48. Keane TJ, Londono R, Turner NJ, Badylak SF. Consequences of ineffective decellularization of biologic scaffolds on the host response. Biomaterials. 2012; 33(6):1771–81. [PubMed: 22137126]

## Appendix. Supplementary material

Supplementary data associated with this article can be found, in the online version, at doi: 10.1016/j.biomaterials.2011.12.055.

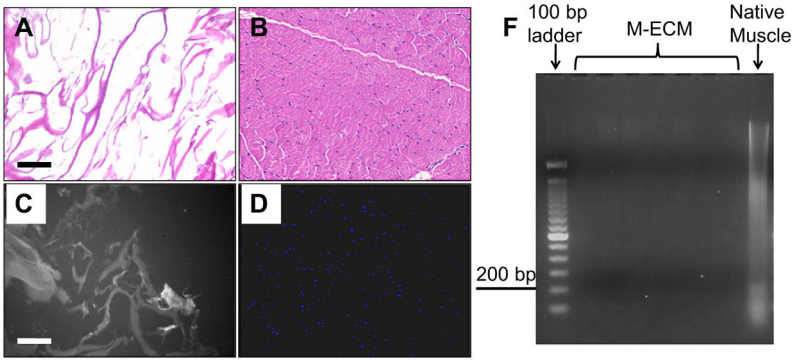


E

| | ng DNA/mg ± SD |
|---|---|
| M-ECM | 7.42 ± 1.67 |
| Native muscle | 1549 ± 489 |

**Fig. 1.**

Residual DNA content of M-ECM scaffolds after decellularization for each batch tested in the study ($n = 7$) compared to native muscle ($n = 2$). Histologic appearance after H&E staining of (A) M-ECM and (B) native muscle tissue, and after DAPI staining of (C) M-ECM and (D) native muscle, bar represents 100 μm. The DAPI stained M-ECM is overexposed and imaged multispectrally displaying scaffold autofluorescence as gray and nuclei as blue. (E) Results of the PicoGreen analysis for double stranded DNA extracted per mg dry weight of scaffolds ± SD. (F) Extracted DNA from several batches of M-ECM separated via 2% agarose gel electrophoresis and compared with native muscle and a 100 bp ladder. (For interpretation of the references to color in this figure legend, the reader is referred to the web version of this article.)

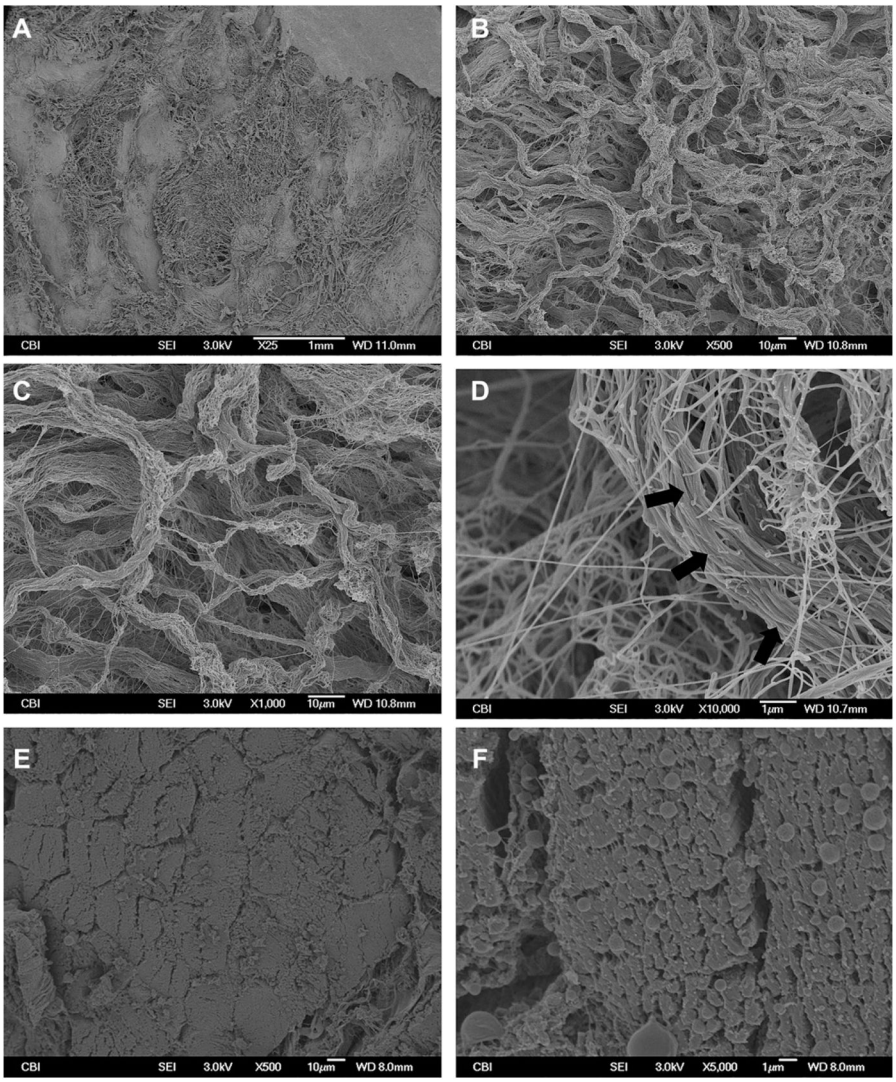


**Fig. 2.**

SEM images of M-ECM and native muscle tissue. M-ECM was imaged at (A) 25×, (B) 500×, (C) 1000×, and (D) 10,000× magnifications and compared to native muscle cross sections at (E) 500× and (F) 5000×. Long fibrils with a collagen-like banding pattern were observed in the M-ECM scaffold.

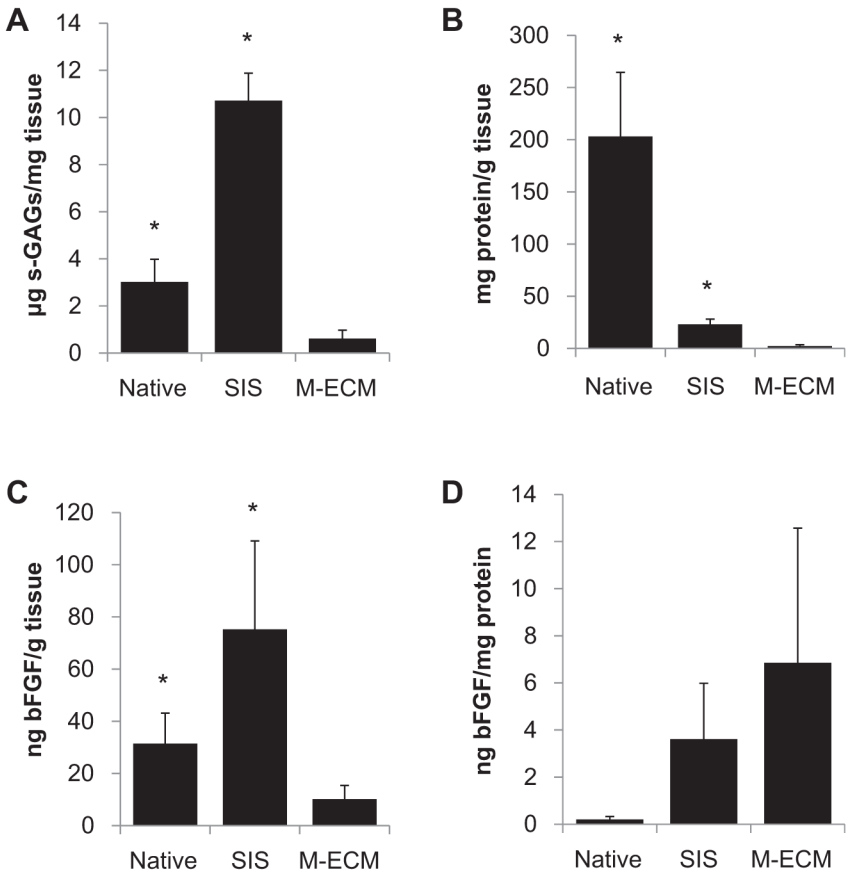


**Fig. 3.**

Biochemical analysis of M-ECM scaffolds ($n$ = 5–7) compared to SIS ($n$ = 3–4) and native muscle tissue ($n$ = 2–3) displaying (A) the sulfated GAG content, (B) total protein recovered after urea-heparin extraction, and (C–D) basic FGF content. (C) displays the total bFGF extracted per initial dry weight of tissue and (D) displays that same amount normalized to total soluble protein extracted.

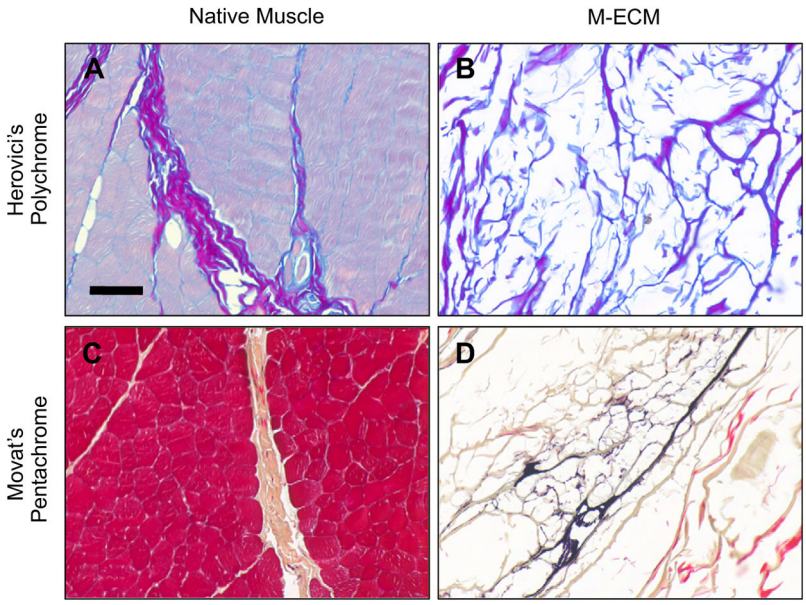


**Fig. 4.**

Histologic appearance after (A–B) Herovici's Polychrome and (C–D) Movat's Pentachrome stains for (B,D) M-ECM and (A,C) native muscle tissue. Scale bar represents 100 μm.

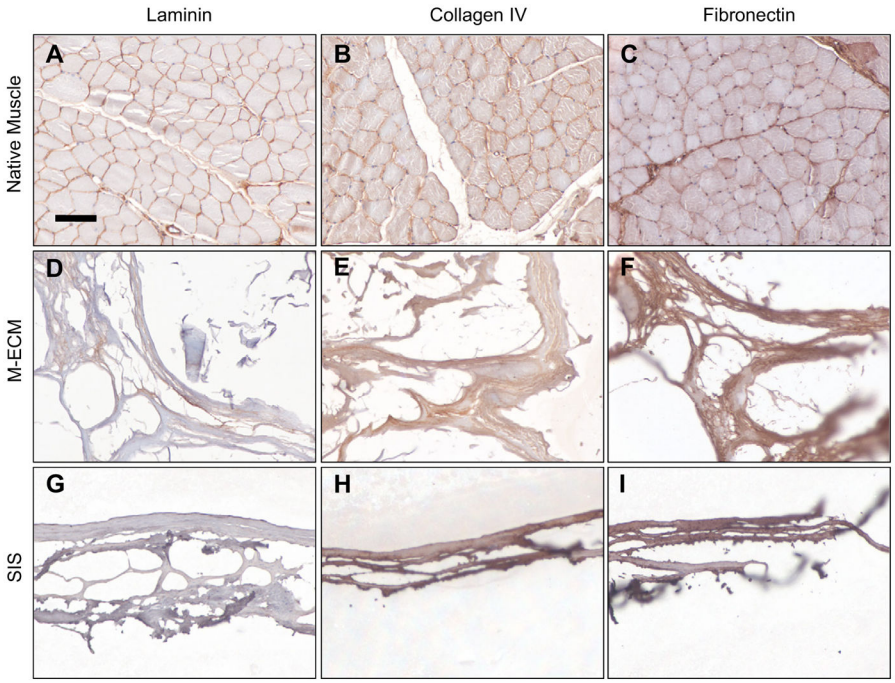


**Fig. 5.**

Immunolabeling of (A–C) native muscle, (D–F) M-ECM, and (G–I) SIS for the basement membrane proteins (A,D,G) laminin, (B,E,H) collagen IV, and (C,F,I) fibronectin. Scale bar represents 100 μm.

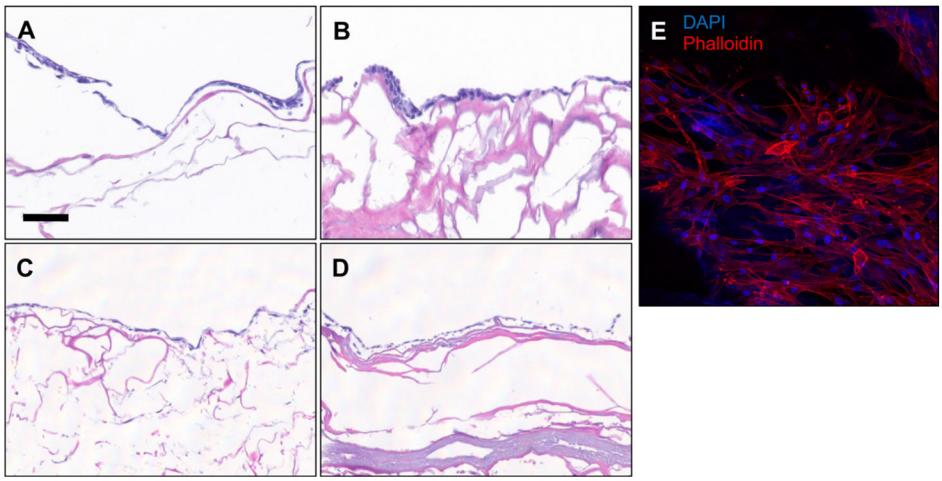


**Fig. 6.**

*In vitro* cell compatibility histology of (A,C) C2C12 myoblasts and (B,D,E) perivascular stem cells cultured for 7 days on the surface of M-ECM (A,B,E) or SIS (C,D). Representative images of (A–D) H&E cross sections and (E) fluorescent imaging labeling with phalloidin for actin (red) or DAPI for nuclei (blue). Scale bar represents 100 μm. (For interpretation of the references to color in this figure legend, the reader is referred to the web version of this article.)

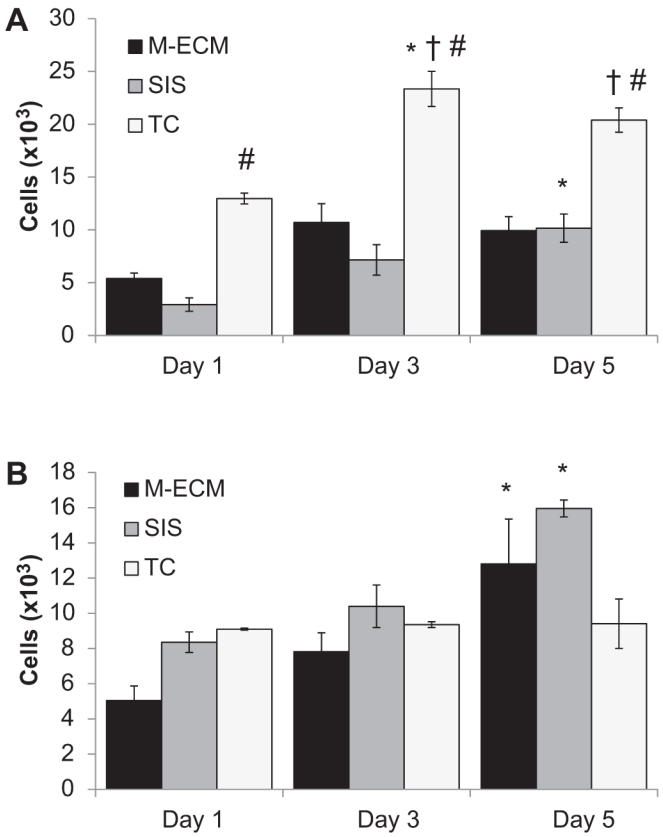


**Fig. 7.**

Alamar Blue assay for cellular metabolism of (A) C2C12 myoblasts and (B) perivascular stem cells seeded on the surface of M-ECM sheets, SIS sheets, or tissue culture plastic (TC) controls for 1, 3, and 5 days. Results normalized to standard curve of cells assayed on TC 4 h after seeding. Significance defined as $p < 0.05$ and * denotes a difference from day 1 within a group, # denotes a difference from SIS within a timepoint, and † denotes a difference from M-ECM within a timepoint.

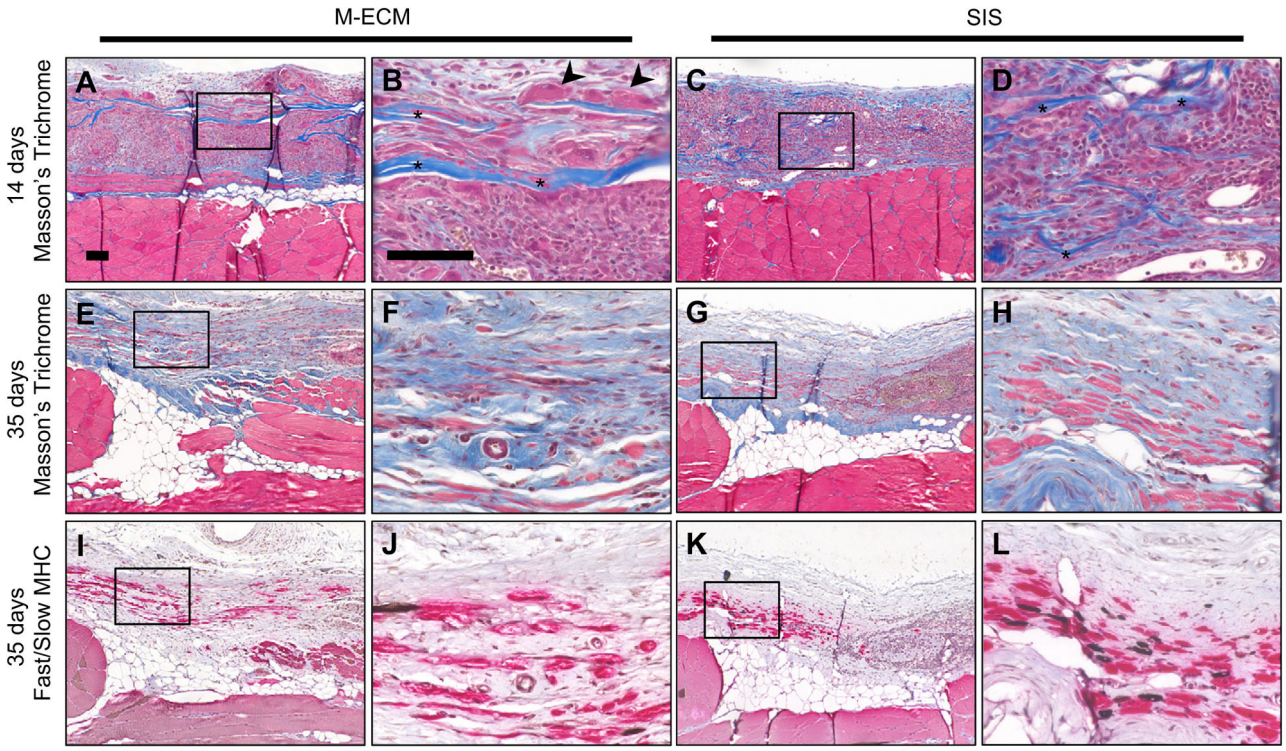


**Fig. 8.**

*In vivo* response to implanted (A–B,E–F,I–J) M-ECM and (C–D,G–H,K–L) SIS after (A–D) 14 and (E–L) 35 days. Sections stained with (A–H) Masson's Trichrome or (I–L) immunolabeled for fast (red) and slow (brown) myosin heavy chain (MHC). There are obvious scaffold remnants at 14 days for both scaffolds (asterisks), and multinucleate cells around M-ECM scaffold regions (arrowheads). Scale bar represents 100 μm. (For interpretation of the references to color in this figure legend, the reader is referred to the web version of this article.)

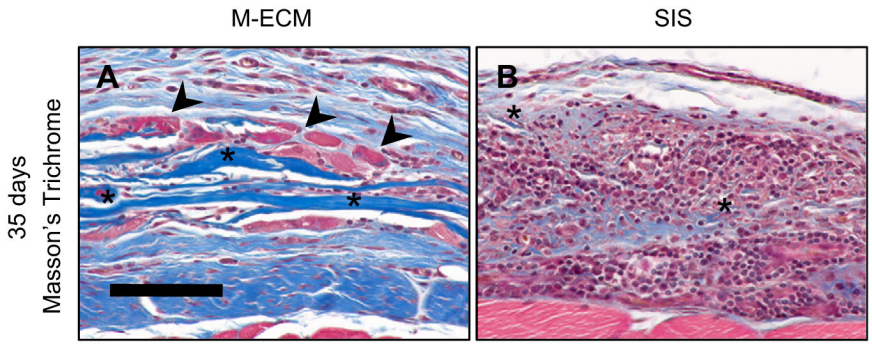


**Fig. 9.**

Areas of incomplete (A) M-ECM and (B) SIS scaffold degradation after 35 days *in vivo* after Masson's Trichrome staining. Scattered M-ECM scaffold remnants (asterisks) are apparent in some regions of the defect, but such regions are smaller and more diffuse for SIS. M-ECM scaffold remnants are also associated with multinucleate cells (arrowheads). Scale bar represents 100 μm.

**Table 1**

Summary of the steps in the decellularization of skeletal muscle tissue including the chemical treatment and time of exposure.

| Chemical | Length of treatment |
|---|---|
| Chloroform/methanol (2:1 v/v) | 2 h |
| Graded series of alcohol (100,90,70,50,0) | 30 min ea. |
| 0.2% Trypsin/0.2% EDTA at 37 C | 2 h |
| Deionized water, 2× PBS | 30 min ea. |
| 2% sodium deoxycholate | 5 h |
| Deionized water, 2× PBS | 30 min ea. |
| 2% sodium deoxycholate | 14–16 h |
| 1% Triton X-100 | 1 h |
| Deionized water | 30 min |
| 0.1% (w/v) peracetic acid/4% ethanol (v/v) | 2 h |
| 1× PBS | 30 min ea. (twice) |
| Deionized water | 30 min ea. (twice) |